The Seventeenth International Symposium on Artificial Life and Robotics 2012 (AROB 17th '12),
B-Con Plaza, Beppu, Oita, Japan, January 19-21, 2012

Stability of Two-Wheeled Mobile Robot Using New Combined Pole-placement Method

Yoko Amano[1]

[1] Nihon University, Koriyama, Fukushima, 963-8642, Japan
(Tel: 81-24-956-8796, Fax: 81-24-956-8796)
(amano@ee.ce.nihon-u.ac.jp)

Abstract: In order to guarantee robotic stability, a new combined pole-placement method is proposed in this paper. The proposed method combines the linear quadratic regulator (LQR) into the pole-placement design. Firstly, a mathematical model of Two-Wheeled Mobile Robot (TWMR) is analytically derived from real TWMR. Secondly, the LQR for TWMR model is designed, and optimal poles can be obtained from the designed LQR. Thirdly, selection conditions of the best poles are the following; 1) the guarantee of convergence speed for TWMR system, 2) the number of vibration times for TWMR, 3) saturation evasion of the control input to TWMR's actuators, 4) the ratio of an imaginary part and a real part is carried out near one of selected poles. The pole-placement method selects the best poles than the optimal poles of LQR. Finally, the stability of the proposed method is confirmed by experiment results.

Keywords: inverted pendulum, linear quadratic regulator, pole placement method, two-wheeled mobile robot

1 INTRODUCTION

Two-wheeled mobile robot (TWMR) always exhibits many problems existing in industrial applications, for example, various nonlinear behaviors under different operation conditions, external disturbances, and physical constraints on some variables. Therefore, the task of on-line control of a highly nonlinear unstable has been a challenge for the modern control field. Since the system behaviors of TWMR including actuator dynamics are highly nonlinear, it is difficult to design a suitable control system that realizes real-time control and accurate balancing control at all time.

On the other hand, many research results of TWMR have been applied to various actual problems for designing walking gaits of humanoid robot, robotic wheelchairs, personal transport systems, and so on. Recently, the control problems of TWMR have been intensively studied due to the challenging demand of fast and precise performance. Besides protecting safety of human and robotic operators, the robotic stability is very important research theme at the longest. There have been many studies on the stable problem, for example, sliding-model control [1], fuzzy switched swing-up control [2], and adaptive control [3] are researched on TWMR. But, these controls are very complex and the response time of the mobile robot system is slower.

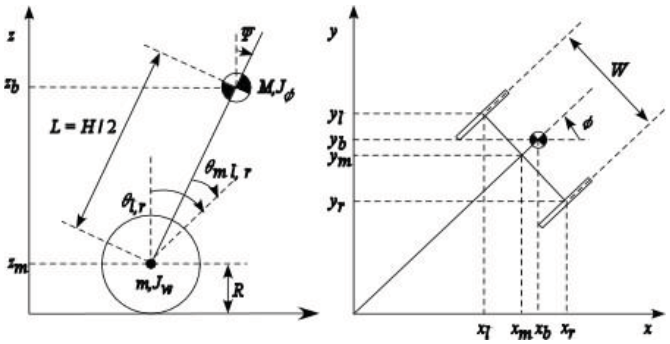

Ψ: body pitch angle, $\theta_{l,r}$: left and right wheel angle,
$\theta_{m_{l,r}}$: DC motor angle
Fig.1 Side and plane view of TWMR

2 TWMR'S MODEL

Figure 1 shows side view and plane view of TWMR, the coordinate system shown in Fig.1 is used TWMR model, and physical parameters of TWMR by measurements are shown in Table 1 [4].

We can drive motion equations from TWMR by the Lagrangian method based on the coordinate system shown in Fig.1, the generalized forces F_θ, F_Ψ, F_ϕ can be expressed

Table 1 Physical parameters of TWMR

Gravity acceleration	g=9.81	(m/sec^2)
Wheel weight	m=0.03	(kg)
Wheel radius	R=0.04	(m)
Wheel inertia moment	J_w=mR^2/2	(kgm^2)
Body weight	M=0.6	(kg)
Body width	W=0.14	(m)
Body depth	H=0.144	(m)
Distance between mass and wheel axle	L=H/2	(m)
Body pitch inertia moment	J_Ψ=ML^2/3	(kgm^2)
Body yaw inertia moment	J_ϕ=M(W^2+D^2)/12	(kgm^2)
DC motor inertia moment	J_m=1 $\times 10^{-5}$	(kgm^2)
DC motor resistance	R_m=6.69	(Ω)
DC motor back EMF constant	K_b=0.468	(V sec/rad)
DC motor torque constant	K_t=0.317	(Nm/A)
Gear ratio	n=1	
Friction coef. of body and DC motor	f_m=0.0022	
Friction coef. between wheel and floor	f_w=0	

using the DC motor voltages v_l and v_r.

$$\begin{aligned} F_\theta &= \left[(2m+M)R^2 + 2J_m + 2n^2J_m\right]\ddot{\theta} \\ &\quad +(MLR - 2n^2J_m)\ddot{\psi} \qquad (1) \\ F_\psi &= (MLR - 2n^2J_m)\ddot{\theta} \\ &\quad +(ML^2 + J_\psi + 2n^2J_m)\ddot{\psi} - MgL\psi \qquad (2) \\ F_\phi &= \left[\frac{1}{2}mW^2 + \frac{W^2}{2R^2}(J_w + n^2J_m)\right]\ddot{\phi} \qquad (3) \end{aligned}$$

here, consider the limit $\Psi \longrightarrow 0$, and neglect the second order term like $\dot{\Psi}^2$.

2.1 State space model

Now, from (1) to (3), we can obtain the following state space model of TWMR.

$$\begin{aligned} \dot{\boldsymbol{x_1}}(t) &= \boldsymbol{A_1}\boldsymbol{x_1}(t) + \boldsymbol{B_1}\boldsymbol{u}(t) \qquad (4) \\ \boldsymbol{y_1}(t) &= \boldsymbol{C_1}\boldsymbol{x_1}(t) \qquad (5) \end{aligned}$$

where, the state variable $\boldsymbol{x_1}(t)$=$[\theta, \psi, \dot{\theta}, \dot{\psi}]^T$, the input $\boldsymbol{u}(t)$=$[v_r, v_l]^T$, and the output $\boldsymbol{y_1(t)}$=$[\theta, \psi, \dot{\theta}, \dot{\psi}]^T$, the parameter matrices of the state space model (4), (5) describe the following.

$$\boldsymbol{A_1} = \begin{bmatrix} 0 & 0 & 1 & 0 \\ 0 & 0 & 0 & 1 \\ 0 & A_1(3,2) & A_1(3,3) & A_1(3,4) \\ 0 & A_1(4,2) & A_1(4,3) & A_1(4,4) \end{bmatrix} \qquad (6)$$

$$\boldsymbol{B_1} = \begin{bmatrix} 0 & 0 \\ 0 & 0 \\ B_1(3,1) & B_1(3,2) \\ B_1(4,1) & B_1(4,2) \end{bmatrix} \qquad (7)$$

$$\boldsymbol{C_1} = \text{diag}\ [1 \quad 1 \quad 1 \quad 1] \qquad (8)$$

$$\boldsymbol{E} = \begin{bmatrix} E(1,1) & E(1,2) \\ E(2,1) & E(2,2) \end{bmatrix} \qquad (9)$$

$$\begin{aligned} A_1(3,2) &= -\frac{gMLE(1,2)}{\det \boldsymbol{E}} \\ A_1(4,3) &= \frac{gMLE(1,1)}{\det \boldsymbol{E}} \\ A_1(3,3) &= -\frac{2\left[(\beta + f_w)E(2,2) + \beta E(1,2)\right]}{\det \boldsymbol{E}} \\ A_1(3,4) &= \frac{2\left[(\beta + f_w)E(1,2) + \beta E(1,1)\right]}{\det \boldsymbol{E}} \\ A_1(4,3) &= \frac{2\beta\left[E(2,2) + E(1,2)\right]}{\det \boldsymbol{E}} \\ A_1(4,4) &= -\frac{2\beta\left[E(1,1) + E(1,2)\right]}{\det \boldsymbol{E}} \\ B_1(3,1) &= \frac{\alpha\left[E(2,2) + E(1,2)\right]}{\det \boldsymbol{E}} \\ B_1(4,1) &= -\frac{\alpha\left[E(1,1) + E(1,2)\right]}{\det \boldsymbol{E}} \\ \det(\boldsymbol{E}) &= E(1,1)E(2,2) - E(1.2)^2 \end{aligned}$$

$$\begin{aligned} E(1,1) &= (2m+M)R^2 + 2J_w + 2n^2J_m \\ E(1,2) &= MLR - 2n^2J_m \\ E(2,1) &= MLR - 2n^2J_m \\ E(2,2) &= ML^2 + J_\psi + 2n^2J_m \end{aligned}$$

$$\alpha = \frac{nK_t}{R_m}, \qquad \beta = \frac{nK_tK_b}{R_m} + f_m$$

2.2 LQR design for TWMR

In this section, LQR design for TWMR is considered as an expansive state space equation. We select θ as a reference state $\boldsymbol{\theta_{ref}}$=$\boldsymbol{C_\theta x_{1ref}}$, and define an error $\boldsymbol{e}(t)$=$\mathrm{C}_\theta \boldsymbol{x}_{1ref}$-$\theta(t)$, $\dot{z}(t) = \mathrm{e}(t)$, then the expansive state space equation can be expressed by

$$\dot{\bar{\boldsymbol{x}}}(t) = \bar{\boldsymbol{A}}\bar{\boldsymbol{x}}(t) + \bar{\boldsymbol{B}}\bar{\boldsymbol{u}}(t) \qquad (10)$$

$$\dot{\bar{\boldsymbol{x}}}(t) = \begin{bmatrix} \dot{\boldsymbol{x}}(t) \\ \dot{\boldsymbol{z}}(t) \end{bmatrix}, \bar{\boldsymbol{A}} = \begin{bmatrix} \boldsymbol{A_1} & 0 \\ 0 & \mathrm{C}_\theta \end{bmatrix},$$

$$\bar{\boldsymbol{B}} = \begin{bmatrix} \boldsymbol{B_1} & 0 \\ 0 & \text{-}\mathrm{C}_\theta \end{bmatrix}, \bar{\boldsymbol{u}}(t) = \begin{bmatrix} \boldsymbol{u}(t) \\ \boldsymbol{x_1}(t) \end{bmatrix}$$

According to an optimal feedback gain matrix $\boldsymbol{K}$ such that the feedback control law

$$\begin{aligned} \bar{\boldsymbol{u}}^*(t) &= -\boldsymbol{K}\bar{\boldsymbol{x}}(t) \qquad (11) \\ &= \begin{bmatrix} -\boldsymbol{k_f} & -\boldsymbol{k_i} \end{bmatrix} \begin{bmatrix} \boldsymbol{x}(t) \\ \boldsymbol{z}(t) \end{bmatrix} \qquad (12) \\ \boldsymbol{K} &= \boldsymbol{R}^{-1}\bar{\boldsymbol{B}}^T\boldsymbol{P} \qquad (13) \end{aligned}$$

minimizes the performance index

$$J = \int_0^\infty (\bar{\boldsymbol{x}}^T(t)\boldsymbol{Q}\bar{\boldsymbol{x}}(t) + \bar{\boldsymbol{u}}^T(t)\boldsymbol{R}\bar{\boldsymbol{u}}(t))dt \qquad (14)$$

subject to the constaint equation (10). Here, matrix $\boldsymbol{P}$ of (13) is the unique positive-definite solution of the associated matrix Riccati Equation

$$\bar{\boldsymbol{A}}^T\boldsymbol{P} + \boldsymbol{P}\bar{\boldsymbol{A}} + \boldsymbol{Q} - \boldsymbol{P}\bar{\boldsymbol{B}}\boldsymbol{R}^{-1}\bar{\boldsymbol{B}}^T\boldsymbol{P} = 0 \qquad (15)$$

As stated above, a servo control for TWMR is shown in Fig.2, where $\boldsymbol{C_\theta}$ = diag $[1, \quad 0, \quad 0, \quad 0]$, and the weight matrices $\boldsymbol{Q}$, $\boldsymbol{R}$ of (13) by experimental trial and error.

$$\begin{aligned} \boldsymbol{Q} &= \text{diag}\ [1 \quad 6\times10^5 \quad 1 \quad 1 \quad 4\times10^2] \qquad (16) \\ \boldsymbol{R} &= \text{diag}\ [1\times10^3 \quad 1\times10^3] \qquad (17) \end{aligned}$$

To calculate the LQR problem, and obtain the gain $\boldsymbol{K}$ is

$$\begin{aligned} \boldsymbol{K} &= [k_\theta,\ k_\psi,\ k_{\dot{\theta}},\ k_{\dot{\psi}},\ k_i] \qquad (18) \\ \boldsymbol{K} &= [-0.867,\ -31.931,\ -1.154,\ -2.783,\ -0.446] \end{aligned}$$

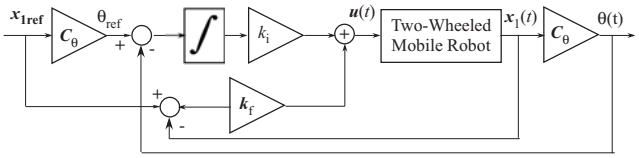

Fig. 2 Servo control system block diagram

3 PROPOSED METHOD

In this section, we present a design proposed method called a combined pole-placement method. We assume that all state variables are measurable and are available for feedback. If the system considered is completely state controllable, then poles of the closed-loop system may be placed at any desired locations by means of state feedback through an appropriate state feedback again matrix.

The present design technique begins with a determination of the desired closed-loop poles based on the transient-response and frequency-response requirements, such as speed, damping ratio, and bandwidth, sa well as steady-state requirements.

3.1 Pole-placement for TWMR

From the expansive state space equation (10) and the optimal control input (11), the closed-loop system can be expressed as

$$\begin{aligned} \dot{\bar{\boldsymbol{x}}}(t) &= \bar{\boldsymbol{A}}\bar{\boldsymbol{x}}(t) - \bar{\boldsymbol{B}}\boldsymbol{K}\bar{\boldsymbol{x}}(t) \\ &= (\bar{\boldsymbol{A}} - \bar{\boldsymbol{B}}\boldsymbol{K})\bar{\boldsymbol{x}}(t) \end{aligned} \tag{19}$$

The desired characteristic equation is

$$\begin{aligned} |s\boldsymbol{I} - \bar{\boldsymbol{A}} + \bar{\boldsymbol{B}}\boldsymbol{K}| &= (s-p_1)(s-p_2)\cdots(s-p_n) \\ &= s^n + a_{n-1}s^{n-1} + \cdots + a_0 = 0 \end{aligned} \tag{20}$$

where, p_i (i=1, 2, $\cdots$, n) are poles of the closed-loop system (19). The first step in the pole-placement design approach is to choose the locations of the desired closed-loop poles. The most frequently used approach is to choose such poles on basis of experience in root-locus design, placing a dominant pair of closed-loop poles and choosing other poles so that are far to the left of the dominant closed-loop poles.

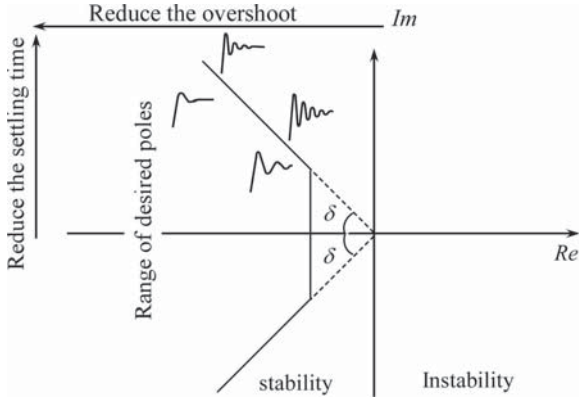

Fig.3 Range of desired poles

We have to note that if the dominant closed-loop poles is far from the $j\omega$-axis, so that the system response becomes very fast, the signals in the system become very large, with the result that system may become nonlinear, this should be avoided and shown in Fig.3.

Another approach is based on LQR approach and determines the desired closed-loop poles such that the system balances between the acceptable response and the amount of control energy required.

In the complex coordinate of Fig.3, an angle $\delta = tan^{-1}(\sqrt{1-\zeta^2}/\zeta)$, here ζ is a damping ratio. For servo control system of robotics, TWMR and so on, $\zeta = 0.6 - 0.8$ and $\delta = 37° - 53°$ have been generally accepted [5].

3.2 Choosing the location of desired closed-loop poles

From $\boldsymbol{K}$ of (18), the pole $\boldsymbol{P_0}$ can be derived and shows the following

$$\boldsymbol{P_0} = [-284.41, -10.92, -1.3 \pm j0.73, -1.47] \tag{21}$$

We change the damping ratio ζ with 0.05 step from 0.6 to 0.8, and obtain poles $\boldsymbol{P_i}$ $(i = 1, \cdots, 5)$ their feedback gains, the ζ and the natural frequency ω_n are shown in Table 2, 3 and 4, respectively.

Table 2 Closed-loop poles

	p_1	p_2	p_3, p_4	p_5
$\boldsymbol{P_0}$	-284.41	-10.9	$-1.3 \pm j0.73$	-1.47
$\boldsymbol{P_1}$	-284.41	-10.9	$-1.3 \pm j0.96$	-1.47
$\boldsymbol{P_2}$	-284.41	-10.9	$-1.3 \pm j1.15$	-1.47
$\boldsymbol{P_3}$	-284.41	-10.9	$-1.3 \pm j1.31$	-1.47
$\boldsymbol{P_4}$	-284.41	-10.9	$-1.3 \pm j1.51$	-1.47
$\boldsymbol{P_5}$	-284.41	-10.9	$-1.3 \pm j1.73$	-1.47

Table 3 Feedback gains

	k_θ	k_ψ	$k_{\dot{\theta}}$	$k_{\dot{\psi}}$	k_i
$\boldsymbol{P_0}$	-0.867	-31.931	-1.154	-2.783	-0.446
$\boldsymbol{P_1}$	-0.927	-32.059	-1.160	-2.797	-0.524
$\boldsymbol{P_2}$	-0.990	-32.191	-1.167	-2.810	-0.604
$\boldsymbol{P_3}$	-1.051	-32.320	-1.173	-2.823	-0.683
$\boldsymbol{P_4}$	-1.138	-32.506	-1.182	-2.841	-0.796
$\boldsymbol{P_5}$	-1.249	-32.741	-1.193	-2.865	-0.939

Table 4 Damping ratio and Natural frequency

	Damping ratio ζ	Natural frequency ω_n (rad/s)
$\boldsymbol{P_0}$	0.87	1.49
$\boldsymbol{P_1}$	0.80	1.62
$\boldsymbol{P_2}$	0.75	1.74
$\boldsymbol{P_3}$	0.70	1.85
$\boldsymbol{P_4}$	0.65	1.99
$\boldsymbol{P_5}$	0.60	2.16

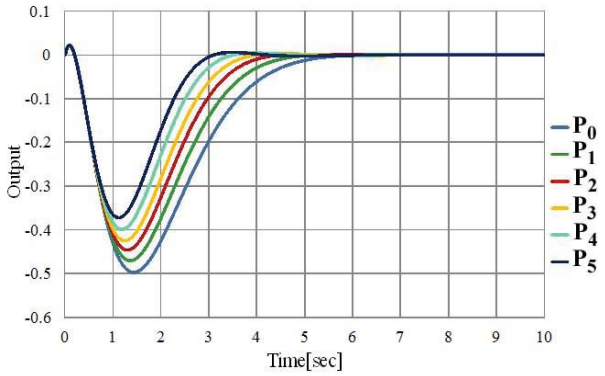

Fig.4 Unit step responses with $\boldsymbol{P_i}$

Figure 4 shows unit step responses of the closed-loop with $\boldsymbol{P_i}$. On the same method, we keep the ζ, and change the real number of the conjugate number $-1.3 \pm j0.73$ with 0.2 step to negative direction. We obtain the good pole $\boldsymbol{P_6} = [-284.4,\ -10.9,\ -1.5 \pm j0.84,\ -1.47]$ with gain margin 5.0 [dB], resonant peak -10.1 [dB], setting time 4.79 (sec.), overshoot -0.41, and $\zeta = 0.87$, $\omega_n = 1.72$ (rad/sec.).

4 EXPERIMENTAL RESULTS

A real TWMR is established practically in our laboratory to illustrate the effectiveness of the proposed method. Using the same parameters shown in Table 1, real stable position experiment is implemented to verify the feasibility of the proposed method with the pole $\boldsymbol{P_6}$ and the LQR method with $\boldsymbol{P_0}$, respectively.

Fig.5 presents the body angle Ψ which tests the stability of TWMR, a small shaking of the body angle with the pole $\boldsymbol{P_6}$ than the pole $\boldsymbol{P_0}$. Fig.6 shows the shifting distance of TWMR at an appointed position. A large distance error using the pole $\boldsymbol{P_0}$ is produced, but, the proposed method with the pole $\boldsymbol{P_6}$ generates very small movement from the appointed position.

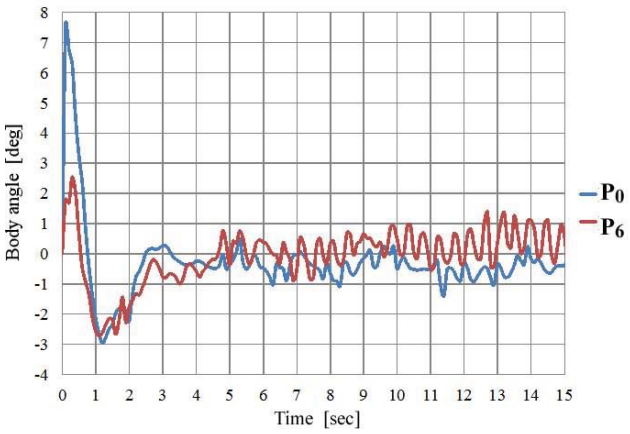

Fig.5 Experimental results of body angle

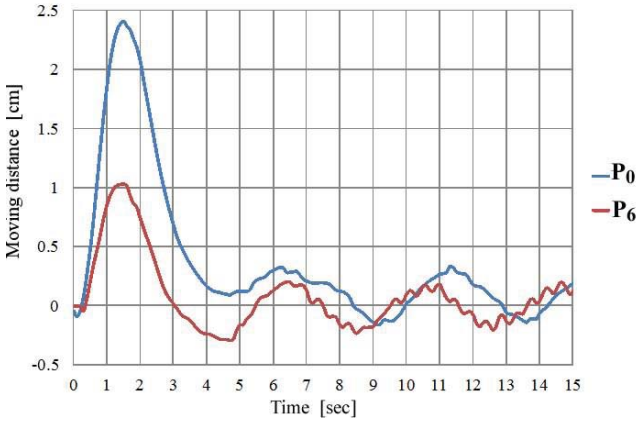

Fig.6 Experimental results of shifting distance

5 CONCLUSION

This paper has implemented the LQR method and pole-placement developmental hardware and software on the real TWMR system, the combined pole-placement method has been newly proposed to control TWMR achieving the desired control behaviors than LQR method.

Finally, the experiment of stable position control was executed using the proposed method and LQR method, the experimental results indeed have verified that the proposed method is effective for the real TWMR system.

REFERENCES

[1] Jian Huang, Zhi-Hong Guan, Takayuki Matsuno, Toshio Fukuda and Kosuke Sekiyama (2011), Sliding-model velocity control of mobile-wheeled inverted-pendulum system, IEEE Trans. Robotics, Vol.26-4, pp. 750-758

[2] Chen-Hao Huang, Wen-June Wang and Chih-Hui Chiu (2011), Design and implementation of fuzzy control on a two-wheel inverted pendulum, IEEE Trans. Ind. Electr. Vol. 58-7, pp. 2988-3001

[3] Zhijun Li and Jun Luo (2009), Adaptive robust dynamic balance and motion control of mobile wheeled inverted pendulums, IEEE Trans. Contr. Syst. Technol. Vol. 17-1, pp. 233-241

[4] Yorihisa Yamanoto (2009), NXTway-GS model-based design, Report of Cybernet systems CO., LTD

[5] Katsuhiko Ogata (2008), MATLAB for Control Engineers, Prentice Hall